ICARUS 28, 247–268 (1976)

Martian Atmospheric Water Vapor Observations: 1972–74 Apparition

EDWIN S. BARKER[1]

The University of Texas, McDonald Observatory, Fort Davis, Texas 79734

Received October 7, 1975; revised January 7, 1976

The patrol of Martian water vapor carried out with the echelle-coudé scanner at McDonald Observatory during the 1972–74 apparition has produced 469 individual photoelectric scans of Doppler-shifted Martian H_2O lines. Almost an entire Martian year was covered during the 1972–74 period (L_s = 118–269° and 301–80°). Three types of coverage have been obtained: (1) regular—the slit placed pole to pole on the central meridian; (2) latitudinal—the slit placed parallel to the Martian equator at various latitudes; (3) diurnal—the slit placed parallel to the terminator at several times during a Martian day measured from local noon.

Both the seasonal and diurnal effects seem to be controlled by the insolation and not the local topography with respect to the 6.1 mb surface. A slight negative correlation with elevation was noted which improved during the seasons of greater H_2O content. The previous seasonal behavior has been confirmed and amplified. The following are the primary conclusions: (1) The planetwide abundance is low (5–15 μm of ppt H_2O) during both equinoctical periods. (2) The maximum abundance of about 40 μm occurs in each hemisphere after solstice at about 40° latitude in that hemisphere. (3) The latitude of the maximum amount in the N–S distribution precedes the latitude of maximum insolation by 10–20° of latitude. (4) During the "drier" seasons (5–20 μm) near the equinoxes on Mars, the atmospheric water vapor changes by a factor of 2–3× over a diurnal cycle with the maximum near local noon. (5) The effects of the 1973 dust storm during the southern summer reduced the amount of water vapor over the southern hemisphere regions to 3–8 μm.

Introduction and History

The coudé spectrographs at McDonald Observatory have been the primary observational source of Martian water vapor since the first systematic observations made by Schorn *et al.* (1967), who reported on observations made during the 1964–65 apparition. They confirmed the detection of water vapor in the Martian atmosphere first announced by Spinrad *et al.* (1963) based on a single coudé spectrogram taken with the Lick Observatory 120-in. (305 cm) telescope. The 1964–65 data were followed by observations primarily at McDonald Observatory during the 1967 apparition, which produced several Martian water plates but none of superior quality due to an unfavorable Doppler-shift maximum during the summer, or wetter, season at McDonald Observatory. During the 1969–70 apparition the presence of water vapor in the Martian atmosphere was confirmed by Schorn *et al.* (1969) and further observations were made by Little (1970) and Tull (1970), giving abundances of 30 to 40 μm during the northern summer season with more water vapor at northern latitudes than at southern latitudes.

Beginning with the second half of the 1969–70 apparition, the observations of water vapor during the southern hemisphere summer season were attempted for the first time. Barker *et al.* (1970) reported the detection of 30 to 50 μm of water vapor

[1] Present affiliation: OAO–PEP Princeton University Observatory, Peyton Hall, Princeton, N.J. 08450.

present during the Martian southern summer season, but were unable to measure a south to north distribution because of the small apparent disk diameter of Mars.

The 1971 apparition did not produce any new information on the seasonal or latitudinal distribution of H_2O vapor. The high-dispersion photographic plate data taken with the 82-in. (208 cm) and the 107-in. (272 cm) telescopes at McDonald Observatory by Barker (1970, 1971) and others for the blue half of the apparition did not obtain any spatial resolution on the Martian water vapor distribution because of very poor seeing during the favorable Doppler-shift period. During the second half of the apparition ($286° < L_s < 21°$),[1] Tull and Barker (1972) observed Martian water vapor for the first time using the Tull coudé scanner on the 107-in. (272 cm) telescope. Using the coudé scannner in the echelle mode, they obtained high-quality photoelectric scans of the Martian water vapor lines for the first time. Unfortunately for seasonal and latitudinal studies, the observational period occurred immediately after the onset of the great 1971 dust storm. Small but detectable amounts of water vapor of 3–8 μm of precipitable water were found to be present in the atmosphere during and immediately after the dust storm. These small amounts would not have been detected by the best photographic spectrum that had been taken previously. The measured abundance increased slightly at the end of the favorable Doppler shift to the 15 μm level at an L_s of 355°. The ground-based measurements over this period agreed quite well with the *in situ* measurements made by the IRIS instrumentation (Hanel *et al.*, 1972) aboard the Mariner 9 spacecraft. A few additional ground-based observations of less than 10 μm were obtained at L_s values of 15 and 21° with a very small planet. With IRIS data taken during the extended Mariner 9 mission at an L_s of 60°, Kunde (1973) and Pearl *et al.* (1974) showed the seasonal increase in the northern spring–summer season to the level of 40 to 60 μm over localized areas.

The data obtained on the presence of water vapor in the Martian atmosphere prior to 1972 are summarized in Table I and Figs. 1 and 2. For uniformity, all abundances have been corrected to the line

[1] L_s is defined as the heliocentric longitude of Mars measured from the Martian vernal equinox and also corresponds to the seasonal periods as on the Earth, with $0° < L_s < 90°$ being spring in the northern hemisphere, etc.

TABLE I

MARTIAN H_2O ABUNDANCE MEASUREMENTS FOR 1964 TO 1972 REDUCED TO FARMER'S (1971) LINE STRENGTHS AT 225 K

Apparition	L_s (°)	Amount (μm)	Location	Reference
1963	76	10		Spinrad *et al.*, 1963 Kaplan *et al.*, 1964
1964–65	5	<11	PPCM	Schorn *et al.*, 1967
	6	<11	PPCM	
	20	<11	PPCM	
	31	<11	PPCM	
	47	~11	PP	
	48	~11	PP	
	49	~11	PP	
	49	~11	PP	
	49	~11	PP	
	50	~11	PP	
	57	~11	PP	

TABLE I—*continued*

Apparition	L_s (°)	Amount (μm)	Location		Reference
	57	~11	PP		
	59	~11	PP		
	60	~11	PP		
	61	~11	PP		
	110	~7	PP		
	112	~7	PPCM		
	114	~7	PP		
	122	~18	PPCM		
1969–70	80	~25	PPCM		Schorn *et al.*, 1969
	111	26	40°N		
		<8	21°S		
	122	26	37°N		
		<8	24°S		
	111	32	PPCM		Little, 1971
		43	N. Polar	54°N	
		24	S. Polar	32°S	
	122	26	N. Equatorial	37°N	
		<10	S. Equatorial	24°S	
	132	40	N. Polar	45°N	
		33	Equatorial	4°N	
		30	S. Polar	39°S	
	132	21	N. Polar	45°N	
		24	Equatorial	4°N	
		<10	S. Polar	39°S	
	134	46	Equatorial	18°N	
	134	49	N. Equatorial	34°N	
		21	S. Equatorial	27°S	
	135	39	N. Polar	44°N	
		<10	S. Polar	40°S	
	136	31	PPCM		
	137	33	PPCM		
	146	29	N. Polar	44°N	
		36	Equatorial	2°N	
		30	S. Polar	40°S	
	120	25	~PP		Owen and Mason, 1969
	132	45	53°N		Tull, 1970, 1971
		46	37°N		
		48	23°N		
		42	11°N		
		35	0°		
		28	11°S		
		21	23°S		
	148	27	46°N		
		30	25°N		
		24	9°N		
		17	9°S		
		11	25°S		
	207	<25	PPCM		Barker, 1971; Barker *et al.*, 1970
	235	13 ± 6	PPCM		
		10 ± 2	~27°N		
		16 ± 6	~33°S		

TABLE I—*continued*

Apparition	L_s (°)	Amount (μm)	Location	Reference
	237	20 ± 6	PPCM	
		14 ± 4	~27°N	
		13 ± 4	~33°S	
	239	14 ± 8	PPCM	Barker, 1971; Barker *et al.*, 1970
		13 ± 8	~28°N	
		16 ± 1	~34°S	
	255	18 ± 4	PPCM	
	279	24 ± 7	PPCM	
	283	27 ± 4	PPCM	
	288	34 ± 10	PPCM	
	289	30 ± 10	PPCM	
		19 ± 3	~6°N	
		14 ± 1	~54°S	
	292	21 ± 4	PPCM	
		16 ± 9	~6°N	
		16 ± 6	~54°S	
	323	38 ± 5	PPCM	
	323	37 ± 10	PPCM	
	323	26 ± 10	PPCM	
	336	37 ± 7	PPCM	
	337	30 ± 10	PPCM	
	339	44 ± 3	PPCM	
1970–71	232	10	TotalDisk	Larson, 1973
	293	10–25	SSolar (Rev 20)	Hanel *et al.*, 1972
	297	5–20	SPC (Rev 30)	
	314	10–20	SSolar (Rev 92)	
	321	5–20	SPC (Rev 116)	
	336	5–15	SSolar (Rev 174)	
	270–360	8	NPC	Kunde, 1973
	60	20–30	N. Hemisphere	Pearl *et al.*, 1974
	90	40–60	Arcadia	Kunde, 1973
	352	1–3	S–N track ±50° latitude	Moroz and Ksanfomaliti, 1972
	358	20	Equatorial	
	286	16.5	PPCM	Tull and Barker, 1972
	285	12.0	PPCM	
	286	10.5	PPCM	
	288	13.5	PPCM	
	299	13.0	PPCM	
	314	18.7	PPCM	
	316	7.5	EQ	
	324	10.8	PPCM	
	327	7.0	PPCM	
	332	6.0	PPCM	
	348	13.0	PPCM	
	350	13.5	PPCM	
	352	14.0	PPCM	
	353	15.0	PPCM	
	353	16.5	PPCM	
	11	9.3	PPCM	Barker, 1974
	21	5.0	PPCM	

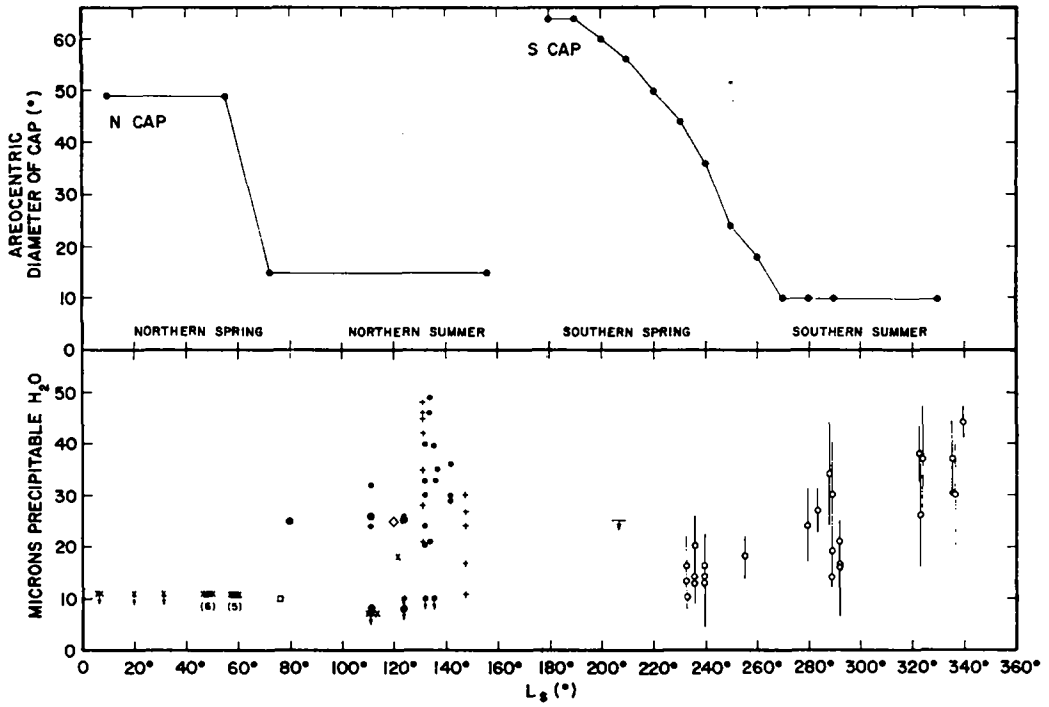

FIG. 1. Measured Martian H_2O abundances from 1963 to 1972. □: Spinrad *et al.*, 1963; Kaplan *et al.*, 1964. ×: Schorn *et al.*, 1967. ⊕: Schorn *et al.*, 1969. ●: Little, 1971. ◇: Owen and Mason, 1969. +: Tull, 1970, 1971. ○: Barker *et al.*, 1970; Barker, 1971. Aerocentric polar cap diameter from Baum and Martin, 1973; Baum, 1971.

strengths of Farmer (1971). Despite all these observations, there still remained parts of the Martian year which had not been covered observationally, particularly those periods during the northern and southern equinoxes. A period of 15 yr is required to fully observe all seasons on Mars from the Earth and then, the lack of a favorable Doppler-shift period may rule out observations during a particular Martian season.

This paper presents the results that were obtained at McDonald Observatory during the 1972–74 apparition which covered the seasonal periods ($118° < L_s < 268°$) and ($309° < L_s < 80°$); consequently, the coverage during this apparition was over almost an entire Martian year.

The observations will be grouped into the three basic types of observational coverage that were made during this period; a seasonal pole-to-pole coverage, a latitudinal coverage or north–south distribution on the planet at any particular season, and a diurnal coverage during two seasonal periods separated by approximately 5 Martian months to measure the diurnal change in the content of atmospheric Martian water vapor over a single day. Preliminary results for the 1972–73 apparition were presented by Barker (1974) for the first half of the apparition. This paper completes the apparition coverage and discusses these apparition data and earlier data sets obtained as a whole to describe the various aspects of the behavior of Martian water vapor.

Observations and Data Reductions

The observations consist of 469 photoelectric spectral scans of the water lines at 8197.704 and 8176.975 Å. The 107-in. (272 cm) telescope has a very large image scale of 2.3 arcsec/mm at f/33 coudé focus which is ideally suited for spatial resolution

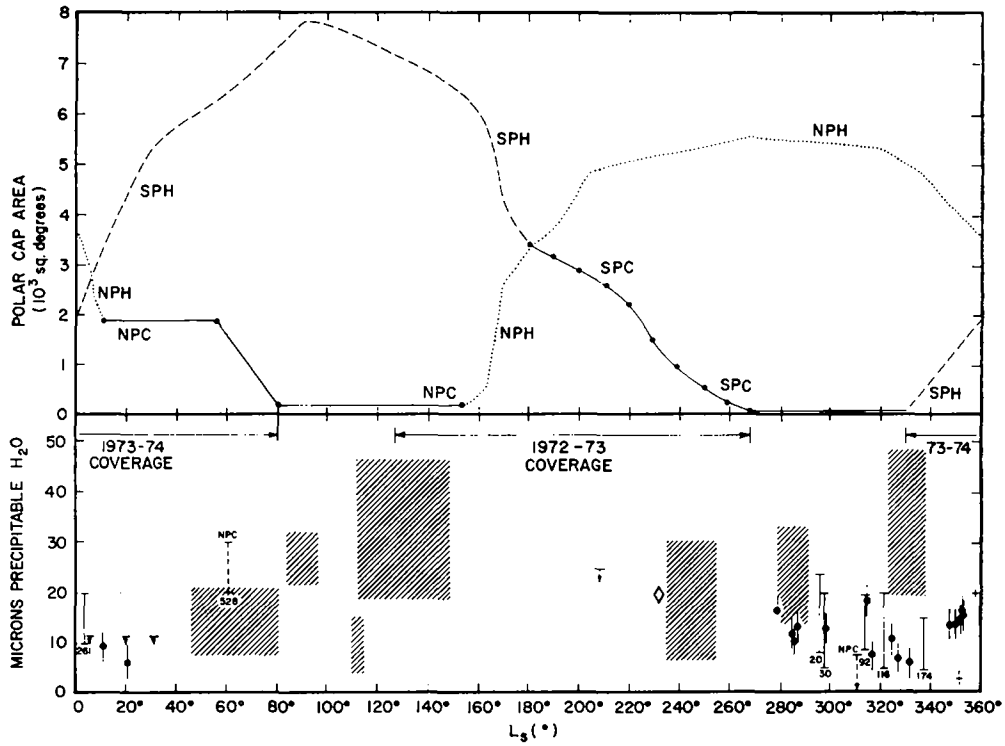

FIG. 2. Measured Martian H_2O abundances for the 1971–72 apparition: ◇: Larson, 1973. I: Mariner 9 data from Hanel *et al.* (1972) with the revolution number attached to the bar; I: Mariner 9 data from Kunde, 1973. +: Mars 3 data from Moroz and Ksanfomaliti, 1972. ♦: ground-based data from Tull and Barker, 1972. The cross-hatched areas refer to data ranges presented in Fig. 1. Surface areas of the polar caps and hoods calculated from Baum and Martin, 1973; Baum, 1974.

studies of atmospheric constituents on planetary disks. The Tull coudé scannner was used in the echelle grating mode, using a 79 groove/mm echelle grating in double pass, which gives a very high dispersion of approximately 8 mm/Å at 8200 Å. The slit-widths for the majority of the Mars water vapor scans have been 200 or 400 μm, giving effective resolution of 30 or 60 mÅ, respectively, at 8200 Å. The entire data acquisition and coudé scanner operation is more fully described by Tull (1972) and Wells (1972).

The acquisition of high quantum efficiency 31034 A RCA Ga As photomultipliers during the fall of 1972 have made these high-resolution photometrically accurate scans possible. The very high quantum efficiency of 10–15% at 8200 Å coupled with a low dark count of 1–2 counts/sec at dry ice temperatures made it possible to obtain a high-precision photoelectric scan of a single line in approximately 30–40 min for Mars. The observations were made whenever the Doppler shift was greater than 0.1 Å, and the planet was larger than 3.9 arcsec. The higher resolution (30 mÅ) was used whenever the Doppler shift was less than 0.23 Å, in order to more fully resolve the Doppler-shifted Martian component of the line being observed.

Most strong water lines in the 8200 Å band are contaminated to some degree by weak Fraunhofer lines "hidden" behind the terrestrial water lines. These Fraunhofer lines are primarily due to CN transitions. All usable water lines (i.e., free from major blends and having observed laboratory line strengths) have been observed on Mercury, using it as a source of variable Doppler shift, to look for hidden Fraunhofer lines. The water lines at 8141, 8193,

and 8256 Å are so seriously blended with solar lines at approximately 1, 2, and 4 mÅ, respectively, that they are not usable for future studies of planetary water vapor. Weak solar lines (<1 mÅ) have been detected and measured in the wings of the 8176, 8189, and 8197 Å water lines. These H_2O lines can be used for water vapor studies, if the solar component of the total Doppler shift does not place them at the Doppler-shifted wavelength of the Mars water vapor lines. It is because of these constraints that we have primarily used the line at 8176.975 Å on Mars during the "blue" part of the 1972–74 apparition and the 8197.704 Å line for the "red" portion of the 1972–74 Martian apparition.

The image rotator was placed in the beam in front of the spectrograph slit so the spectrograph slit could be oriented with respect to the Martian equator or north–south correction by using the values given for the position angle of the axis of Mars obtained from the *American Ephemeris and Nautical Almanac*. A large number of Martian scans were obtained during daylight hours at McDonald Observatory, taking advantage of telescope time not used by other coudé observers during the daylight hours. We substantially increased the seasonal coverage of Martian water vapor without nighttime scheduling of telescope time by using these daytime hours. For the daytime observations a counting rate ratio between the planet plus sky and the sky alone was monitored several times during each scan period. With this measured ratio, an appropriate amount of a solar scan or sky scan over the same wavelength regions at a similar airmass was subtracted from the Martian water vapor scan. The sky contribution to the total signal varied, but was less than 25% of the signal for the majority of the observations. Only for those observations taken at the beginning and end of the apparition when the planet was very small, i.e., near L_s angles of 118 and 80°, did the sky signal exceed that 25% level and then the sky signal was less than the 65% level. To minimize the sky contribution, an entrance decker limited the slit length only to the planetary disk. This entrance decker was also used on occasions to isolate particular portions of the planetary disk used to detect localized observations of Martian water vapor, particularly those observations concerned with the diurnal variations during the morning–evening series.

Each photoelectric scan was processed through several steps to remove the effect of sky background, dark count level, and system vignetting in the echelle system. Any spectrum that did not contain a measurable water line in both the forward and reverse scans was rejected. This was a very small percentage of the data taken and rejection was usually because of electrical pickup noise in one of the scan directions. The final spectrum plot consisted of the data points representing the summation of the forward and reverse scans and a smooth curve drawn through these points as a result of a computer smoothing program based on a fast Fourier transform smoothing operation using the power spectrum of the data to indicate the spatial frequencies above the white noise level. The equivalent widths of the Martian water vapor lines were obtained by measuring the area between the smoothed fast Fourier transform curve and a local continuum curve with a planimeter. The local continuum shape in the wing of the water line had been transferred from a solar scan of similar water content which had been taken on the same observational day or on a day when the water content of the solar scan more closely matched the telluric water content of the Martian scan.

A set of observations for one day consisted of one scan of the entire water vapor line from the blue or red wing of the core well into the continuum to be used for wavelength measurement and continuum placement. Subsequent scans of a shorter wavelength range were centered on the Martian water vapor line. This was done to conserve observing time and obtain higher precision in the photoelectric data.

The digital form of the photoelectric data made computer processing the data almost routine and was completely necessary in terms of the great volume of data involved with this project. The 469 Martian

water vapor scans plus their associated solar, sky, and vignetting scans were processed using an IBM 1800 computer at McDonald Observatory and its associated Houston Instruments plotter. The availability of faster data reduction, in fact sometimes almost instantaneous data reduction, was very superior to the former methods of microdensitometering photographic plates, which on occasions resulted in a lag of weeks before numerical results of a particular observation were known. We could modify our observing program on a day-to-day basis based on the reduction of the previous day's scans, and we did this on several occasions, particularly looking for the latitudinal- and diurnal-type variations.

The guiding on the Martian disk was aided by the use of an RG-5 or RG-2 filter placed in the guiding telescope to improve the contrast against the daytime sky and, more importantly, allow us to guide at a wavelength of approximately 6200 to 6500 Å, which is not significantly different (<0.5 arcsec) from the refracted image at 8200 Å for the great majority of the observations. Also in the focal plane of the guiding eyepiece a graduated reticle with divisions of three-quarters of a second of arc was used to guide on selected fractions of the visible planetary disk. The spatial resolution on the planet was limited in almost all cases by the seeing on the disk of the planet.

Equivalent widths for the Martian water vapor lines were measured by methods described earlier. Assuming a temperature of 225K and Voigt profiles with a value of $a = 0.05$, which corresponds to an effective pressure of 6mb, these equivalent widths were converted into total vertical abundances of precipitable water by using water line strengths at 225K given by Farmer (1971) and the tables of Jansson and Korb (1968). Using methods presented by Woodman and Barker (1973) and using the photometric seasonal map of de Vaucouleurs (1967) instead of a uniform disk, airmass values for each observation and slit position were calculated from Martian physical data and estimates of telluric atmospheric seeing during each observation. This method and its computer program were slightly modified to work with photoelectric data, and

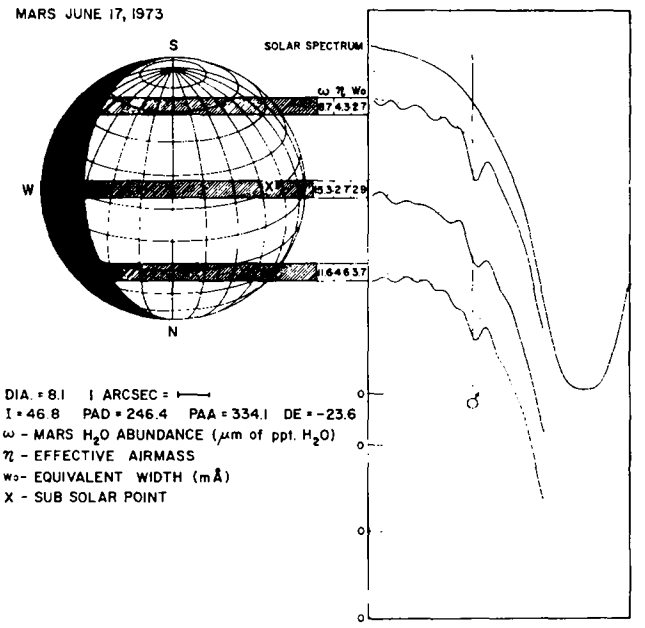

FIG. 3. Typical spectral scans of the 8176 Å line with corresponding slit position on the Martian disk. The slits were placed parallel to the Martian equator at varying fractions of the disk diameter.

proved informative as to different values of the airmass near the terminator (~5.0) and limbs (~2.8) of Mars due primarily to large phase angle (~45°) for Mars.

A typical day's set of observations is shown in Fig. 3, along with a diagram indicating spectrograph slit placement on the disk of Mars. Measured and calculated values of the airmass abundance and equivalent width are given for each slit position. Note that the smaller airmass nearer the center of the disk, unlike the airmass at 1.5 arcsec from the polar limbs, more than compensates for the larger equivalent widths on the polar scans, resulting in a vertical equatorial abundance which is 50% greater than the vertical polar abundances.

Discussion

We can divide the 1972–74 data into three sets: PPCM (pole to pole on the central meridian), EQ (parallel to the Mars equator at various latitudes), and TERM (parallel to the terminator at positions between the limb and the terminator). The slit positions for various fractions of the visual disk are explained in Figs. 3, 4, 7, and 9. Since the three sets describe the seasonal, latitudinal, and diurnal behaviors of the Martian H_2O vapor, the discussion will be separated into these three categories. A tabular listing of physical parameters corresponding to each observation appears, along with the observed equivalent widths and calculated abundances, in tables which are readily available on request from the author. The length of these extensive tables prevented their inclusion in the published version of this paper.

Pole to Pole on the Central Meridian (PPCM)

The greatest coverage in L_s was obtained in the PPCM data presented in Fig. 4, since this slit position was used when the planet was small (~6 arcsec) or the quality of the seeing was not high enough to permit good spatial resolution on the planetary image. The coverage began at $L_s = 118.1°$ and ended almost 1 Martian year later at $L_s = 79.6°$. Because of these observing

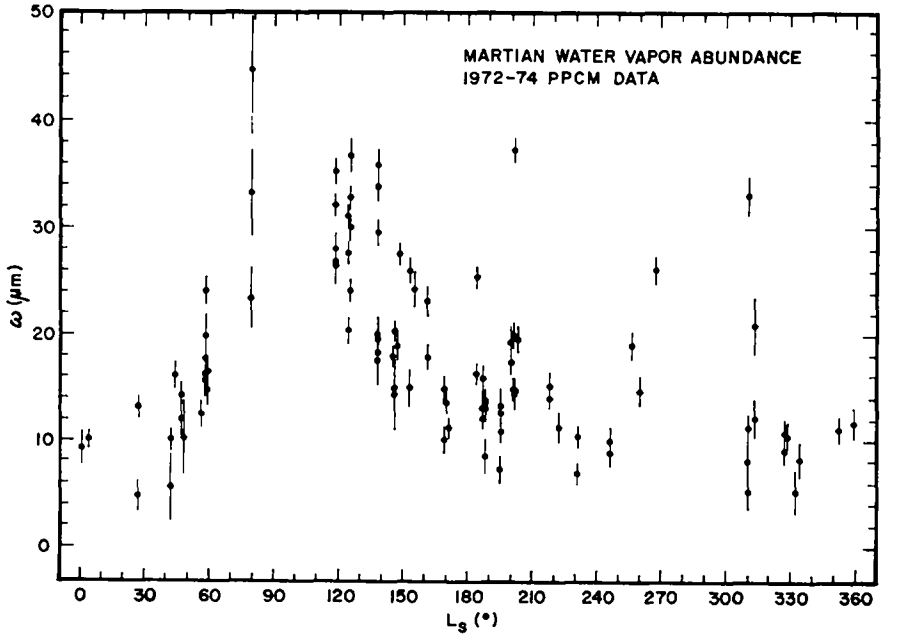

Fig. 4. 1972–74 Mars H_2O abundances for slits placed pole to pole on the central meridian as a function of Martian season, L_s.

factors on the PPCM data, it is the most representative of the planetwide H_2O abundance at any L_s value. Also, these data can be best compared to the high-dispersion photographic spectra because a typical plate exposure allowed Mars to rotate through about 60° of longitude.

During the period from $L_s = 120$ to 240°, the abundance shows a decline from the 35μm range, which is typical for the northern summer season, to a minimum of 8 to 10μm. A marked increase in the PPCM abundance occurs in the next period from $L_s = 250$ to 270°. Based on the spatial data in the equatorial PPCM series, the increase must be coming from the higher (40°) southern latitudes.

The break in the PPCM data from $L_s = 270$ to 310° was caused by the lack of a usable Doppler shift ($\leqslant$0.1 Å). The low abundance observations at $L_s = 310°$ occurred just after the 1973 dust storm began at $L_s = 301°$, again showing, as did the 1971 dust storm, the lack of atmospheric H_2O after or during a major dust storm. With the exception of the data taken at $L_s = 311°$ over higher elevations on the planet, the PPCM abundance remained low, near 10μm, until $L_s = 45°$, when the northern increase in the H_2O vapor began to occur. This increase continued up to $L_s = 80°$ to the 3μm level. Unfortunately, the planet became too small (<3.8 arcsec) and too faint to observe against even the best daytime sky background after $L_s = 80°$.

The PPCM data presented in Fig. 4 confirm the observed, pre-1972 behavior of Martian H_2O except for the period of $L_s = 270$ to 350° because of the 1973 dust storm effects. These planetwide measurements of the H_2O abundance are further amplified and complemented by the large body of scans taken with good spatial resolution described in the next section.

Equatorial Abundances (EQ)

For the equatorial data set, the spectrograph slit was placed parallel to the Martian equator at various fractions of the polar disk diameter. The number of fractions into which the disk diameter was divided depended on the seeing and the total disk diameter for each day of observation. The slit placement on the disk of Mars corresponded to an effective Martian latitude which has been tabulated along with the other physical parameters for each EQ scan. The range covered in latitude was approximately ±10°, but the actual uncertainty depended on the seeing, placement, and guiding errors.

The EQ abundances behave similarly to the PPCM abundances over the Martian year, particularly the decrease from the 35μm value during late northern summer to a minimum value in midspring in the southern hemisphere around $L_s = 230$ to 240° of 5 to 10μm. A sharp increase occurs between $L_s = 260$ to 270° to the 30μm level over the higher southern latitudes. As did the PPCM abundances, the EQ abundances were low (5 to 7μm) after the onset of the 1973 dust storm. The southern half of the disk remained low (<10μm) until $L_s = 50$ to 60°, with the northern half of the disk slightly higher (10 to 20μm) and more variable up to $L_s = 50°$. Between $L_s = 30$ and 60°, the northern half of the disk increased to the 30μm level, while the southern half remained low (5 to 10μm)

All the observed scatter is real, considering that the internal errors in the abundance determinations are small (1 to 2μm). However, a large portion of this scatter. can be removed by plotting the EQ abundance versus the actual planetary latitude of the observation and dividing the EQ data set into L_s regions of similar overall H_2O behavior. The observed H_2O distribution for each individual day of observation is shown in Fig. 5. We have connected observations taken on the same day at different latitudes by solid lines. The slit positions of fractions of the polar diameter have been converted into effective latitudes for the center of the slit. Usually the width of the slit corresponded to 20° or less of planetary latitude, but not less than 10°.

During the nine periods of L_s, the evolution of the polar regions is noted by the latitudes and direction of movement of the polar cap or polar hood boundaries (Baum and Martin, 1973; Baum, 1974) during the

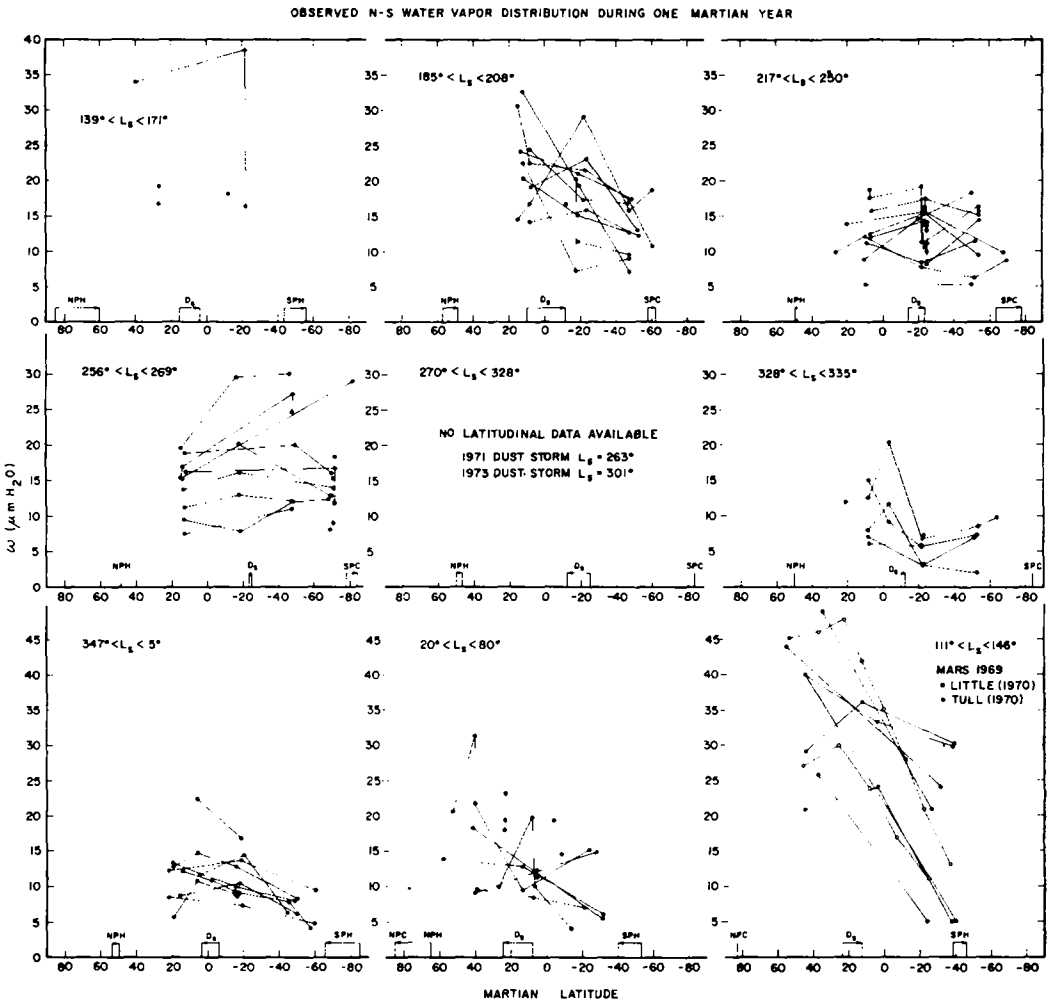

FIG. 5. Observed latitudinal H_2O distributions during nine different seasonal periods. Solid lines connect observations made on a single day.

L_s period along with the movement of the latitude of the subsolar point D_s.

In the 1972–74 data set, we could not observe the H_2O distribution during the $111° < L_s < 146°$ period because of the lack of image scale and during $270° < L_s < 328°$ due to the dust storms in 1971 and 1973 in the southern summer season. Fortunately, the best photographic data, that of the 1969 opposition, had good latitudinal coverage during the $111° < L_s < 146°$ period. The data of Tull (1970) and Little (1971) have been used to fill this period, although their intrinsic measurement errors ($\pm 10\mu m$) are at least three times those of the photoelectric data. Hopefully, in mid-1975, we can obtain coverage of the $270° < L_s < 328°$ period without a Martian dust storm occurring to affect the H_2O abundance.

To isolate the trends of the H_2O distribution for each L_s period from the local weather, we have taken means over 10° bins in latitude when abundance measurements were available. The mean H_2O abundance distributions appear in Fig. 6, with the dashed lines indicating less than three samples in the mean value for a 10° latitude bin. The error bars refer to the standard deviation of the mean value for

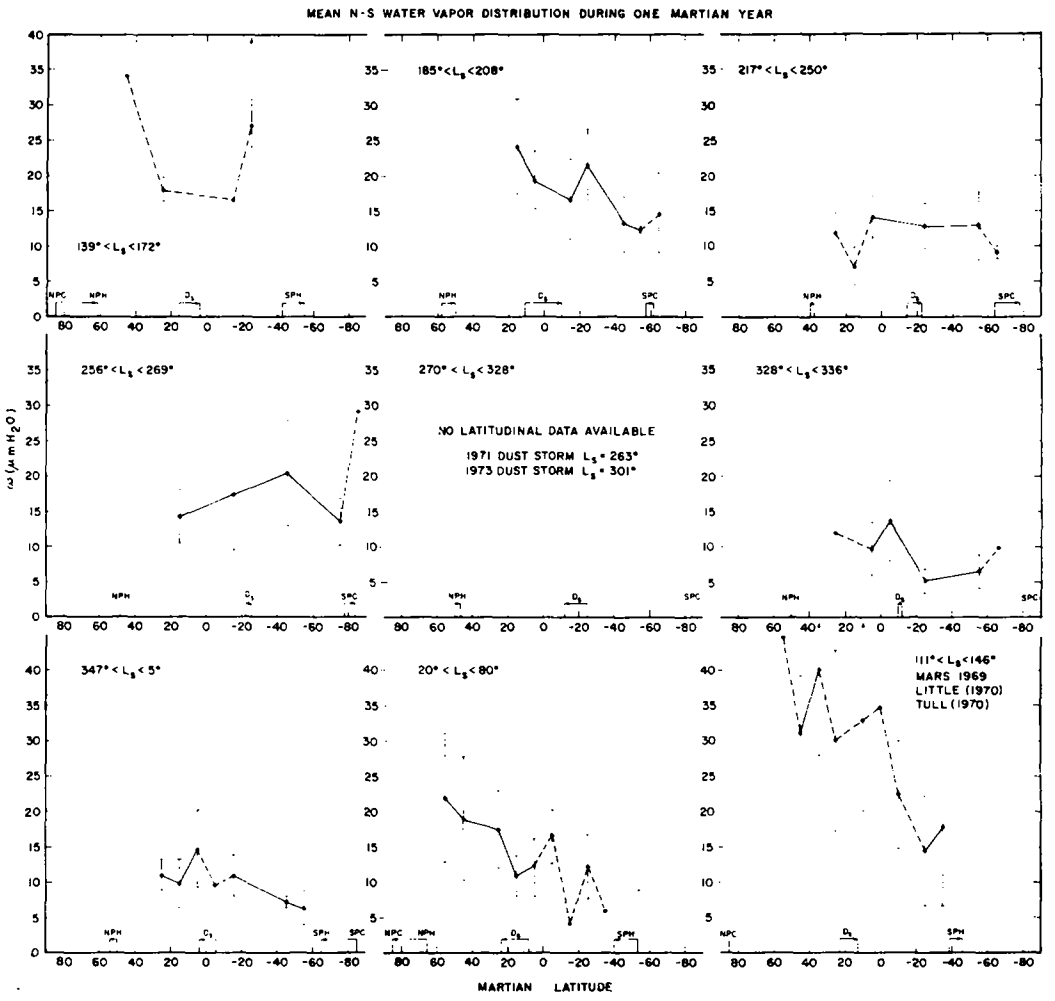

FIG. 6. Mean latitudinal H_2O distribution during the Martian year.

each bin. A general description of the H_2O behavior during the nine L_s periods follows.

$139° < L_s < 171°$. The number of points is small (6) because of the lack of image scale during the first observational period of the 1972–74 apparition. The general trend is toward lower abundances in the southern hemisphere. This L_s range overlaps with the ninth period $111° < L_s < 146°$, when the spatial coverage was good during the 1969 apparition.

$185° < L_s < 208°$. A very strong decrease of almost a factor of 2 occurs between midnorthern latitudes and regions near the edge of the south polar cap which is moving further south. The two observations near the northern edge (~60°S) of the south polar cap were made at an L_s of 208°. Abundances measured 2 Martian months later at this same latitude of 60°S were still at the same 13 to 15 μm level. The apparent increase at 20°S is interesting since this latitude is about 20° south of the subsolar latitude, D_s.

$217° < L_s < 250°$. The north polar hood has reached its stationary or maximum size and the entire planetwide H_2O abundance is low. No N–S trend is noted with the abundance decrease from the previous L_s range taking place only in the northern latitudes. The south pole cap continues to

recede, with a marginally significant lower abundance noted near its boundary.

256° < L_s < 269°. This period terminated because of the lack of a sufficient Doppler shift after $L_s = 270°$ in 1973. The trend toward larger abundances in the midsouthern latitudes is evident, but near the edge of the polar cap, the abundance is still low. The single point at 81°S of 29 μm was taken at an L_s of 268° and may be just an indication of larger abundances by this season. Observations at $L_s = 262°$ were made on the same terrestrial day over the south polar cap and the region immediately north of the edge of the southern cap. The abundance values of 16.6 ± 0.8 and 11.9 ± 1.2 μm, respectively, are not significantly different, considering the possible errors in the guidance and the air-mass calculations.

270° < L_s < 328°. This range of L_s does not have any observations with sufficient image scale or under nondust conditions to determine a N–S H_2O distribution. On the basis of whole-planet data observed in 1969 of 21 to 44 μm, and similar behavior between northern and southern summer seasons, we would expect to find at least twice as much H_2O vapor at 50°S as at +20°N for this southern summer season. Unfortunately, we have been severely hampered by planetwide dust storms during 1971 and 1973 which have occurred during this seasonal period. The 1969 observations were not contaminated by a dust storm (Capen, 1971, 1972, personal communication). H_2O observations during and after the 1971 and 1973 dust storms indicate very low H_2O abundances of 5 to 10 μm, probably resulting from the removal of the H_2O vapor by adsorption onto the dust grains since the observed abundances did not increase when the dust storm cleared.

328° < L_s < 335°. This L_s range corresponds to the period after the 1973 dust storm cleared. The southern latitudes still have a very low abundance of 3 to 8 μm, indicating that the H_2O vapor is still masked or has been removed by the dust storm, which was strongest over these latitudes (Capen, 1974). The H_2O abundance may be higher over the subsolar region and there may be a slight increase toward the northern latitudes. The shape of this distribution continues into the next range of L_s, when the atmosphere was free of the dust storm.

347° < L_s < 5°. The entire planet is low with a slight increase toward northern latitudes and an increased level over the subsolar region. Since the atmosphere was clear by this time, the H_2O must have been removed from the southern latitudes during the dust storm. The south polar hood has started to form by the end of this range. This seasonal period is similar to the $185° < L_s < 208°$ season for the northern hemisphere. In the absence of a southern hemisphere dust storm, the abundance in the southern latitudes (0 to 50°S) would have been 15 to 25 μm.

20° < L_s < 80°. During this range, a marked increase in the H_2O abundance occurs between 20 and 60°N, with the 20°S region remaining low. This pattern is just reversed from that seen in the $217° < L_s < 269°$ period for the high southern latitudes. Due to the small image size by $L_s = 60°$, we could not say that the increase occurred above 40°N or over the subsolar point. The northern polar hood has disappeared and the northern cap has receded to its minimum size during this season.

111° < L_s < 146°. We have used the 1969 plate data to fill in the coverage of the N–S H_2O distribution. Since the plate data were long exposures (about 4 to 6 hr, corresponding to 60 to 90° longitude), there is a much greater averaging effect on local concentrations of H_2O vapor. The data presented by Tull (1970) have the best spatial resolution, which shows a maximum over the subsolar latitude in addition to the decrease from north to south. The low points on Fig. 1 are those plates measuring primarily the abundance in the southern latitudes (20°S).

In conclusion, Fig. 6 shows the mean latitudinal distribution of Martian water vapor over a Martian year and its dependence on the surface and atmospheric temperature as defined by the N–S movement of the subsolar latitude. The maximum amount of water vapor at all seasons is at the subsolar latitude of a few degrees

(10 to 20°) north or south of that latitude in phase with the direction of the N–S motion of the subsolar latitude.

Diurnal Abundances (TERM)

Two sets of special observations, approximately 5 Martian months apart, were made during periods in the Martian seasons when there was about 10 to 20 μm of precipitable water above the equatorial regions. These periods were seasons when the water vapor abundance on Mars was relatively low. We obtained measurements both during the evening-terminator, morning-limb period of time (Barker, 1974) and the morning-terminator, evening-limb period of time. Observations were made by placing the spectrograph slit parallel to the terminator line near the terminator and limb and at the center of the visible disk. These slit positions are illustrated in Fig. 7.

We sampled areas on the Martian disk with approximately the same local time along the slit and, hence, the same diurnal temperature phase along the slit. Due to the large phase angle of about 45° during the observing periods, the subsolar point was under the limb scan most of the time. The slit positions in the evening terminator series approximately referred to: limb to midday; center of the visible disk to mid-afternoon; and terminator to late evening. Likewise, the morning terminator slit positions referred to: terminator to early morning, center of the visible disk to mid-morning and limb to midday. Since slit placement was critical, all diurnal H_2O vapor observations were made when the seeing was 2 arcsec or better (*usually* 1 arcsec).

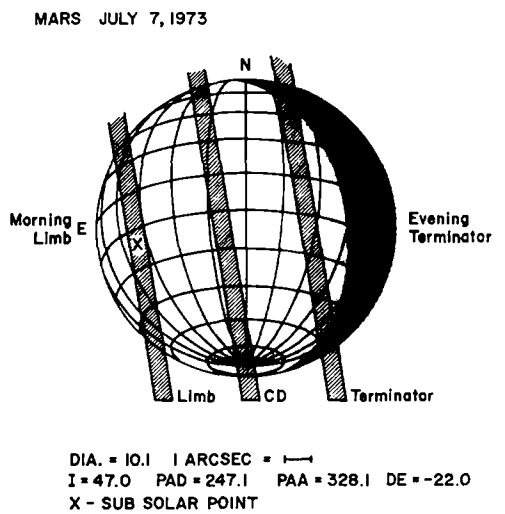

FIG. 7. Schematic representation of the actual slit positions for the evening terminator series diurnal data obtained on July 7, 1973. The slit was oriented parallel to the terminator line at the center of the disk, 1½ arcsec in from the limb and 1 arcsec in from the terminator.

Using the computer program developed by Woodman and Barker (1973), the geometrical airmass factor was calculated for each slit position subtended on the planet. This correction was very necessary because of the large airmass values (4 to 5) near the terminator. When the geometrical airmass factor is removed from the observed abundance, we obtain the abundance (ω) plot shown in Fig. 8 which is the vertical or unit abundance of water vapor above a certain location on the planet. Observations taken within about 2 to 3 hr on the same day are connected with straight lines, with a few points being means of measurements made an hour apart. The size of the Martian disk governed the spread of local times, which we were able to sample on a given date. When the disk was greater than 12 arcsec, we were able to divide it into five slits rather than the three positions which were obtained on the majority of days. Although there is a large amount of scatter in the vertical abundance plot, the general trend of all the lines leads one to conclude that there is a decrease of a factor of 2 in the amount of water vapor in the evening with respect to the amount seen at midday for the evening terminator series.

In Fig. 9 the orientation of the slits used in the morning terminator series is illustrated. To minimize the effects of the lower temperatures in the polar regions, we shortened the slits to one-half the disk diameter, which restricted them to the sub-Earth latitudes. The terminator corresponded approximately to 0730 in the morning; the center of the visible disk, to

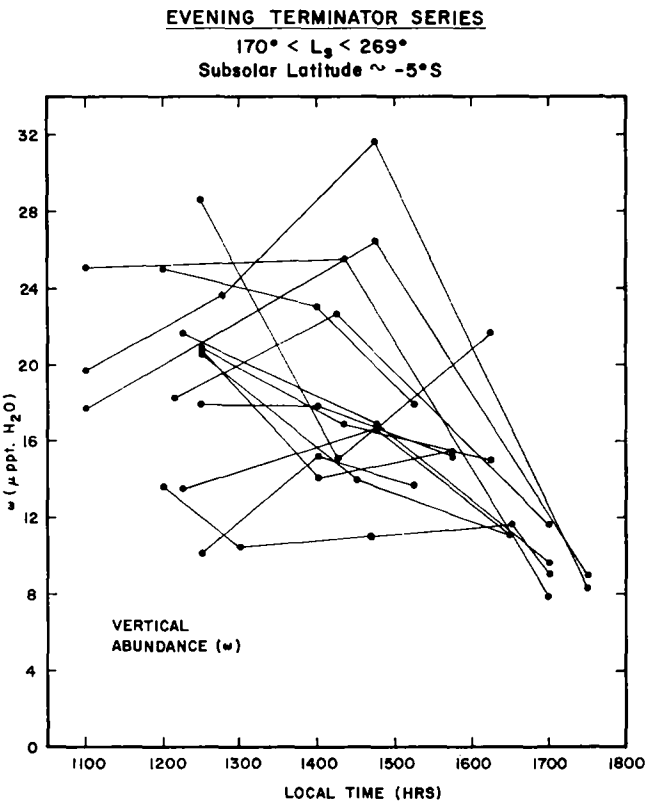

FIG. 8. Vertical abundances for the evening terminator series.

1015; and the limb again, to midday or about 1215.

When the geometrical airmass factor is applied to the morning terminator observations, the vertical abundance shown in Fig. 10 is systematically lower at the morning terminator, 0700hr in the morning, local time, increasing to a maximum around 1200hr. The reason for the decrease at 1300 is that three sets of observations taken at this time of day were 3 to 5μm lower than the mean level, probably because of the remaining effect of the 1973 dust storm. The maximum abundance does not reach the 20μm level, as it did for the evening terminator series, because of the lower amount of water vapor in the Martian atmosphere during the morning terminator series; also, it may be a function of the October 1973 dust storm on Mars. Unfortunately, ground-based observations of the morning and evening terminator abundances are not possible during the same seasonal period on Mars.

In Fig. 11 we have the mean diurnal variation of water vapor for the morning and evening terminator series. For completeness, one should treat each set of observations separately, using the temperature profiles that match the season, local topography, subsolar latitude, etc., but to see how the water vapor behaves in general, we have taken means of the observed diurnal variations of the vertical abundances presented in previous figures. These means are over 1hr intervals centered on the half-hour, when sufficient data were available. In general, we find that the water vapor increases from 5μm at 0700hr to a noon maximum of 13μm for the morning terminator series. The evening terminator series has a higher abundance

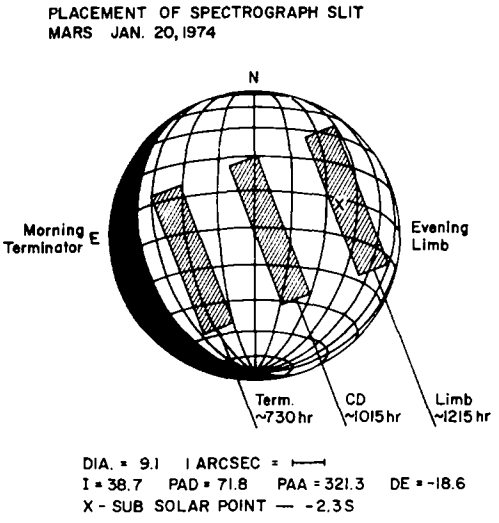

FIG. 9. Schematic representation of the actual slit positions for the morning terminator series obtained on January 20, 1974. The length of the slit was set at one-half the disk diameter.

during the noontime period of about 21 μm, which decreases to a minimum of 9 μm in the late evening at 1730 hr.

At this point it is appropriate to ask what could cause a systematic lower or higher abundance in the Martian atmosphere. First, we could say that there is weather present in the Martian atmosphere. This is probably true and is a contributing factor to the scatter in the data presented in Figs. 8 and 10. Second, local topography, albedo, or surface features may produce systematically higher or lower water abundances. Since we have sampled most of the central meridians of Mars with both the diurnal and PPCM data sets and see no systematic abundance variations as a function of longitude of the central meridian, we can discount this explanation.

Temperature variation in the Martian atmosphere on a diurnal cycle is the most likely explanation of any change in the water vapor abundance. If an isothermal atmospheric layer at temperature T_0 (~225 K) contains 20 μm of water vapor at or near saturation, a temperature change only of $\Delta T = -11$°C decreases the 20 μm to an observed abundance of 10 μm. Also, if that 20 μm was not at saturation but was at a relative humidity of 10%, a temperature change of only $\Delta T = -28$°C would reduce this abundance to 10 μm. The question is whether such diurnal

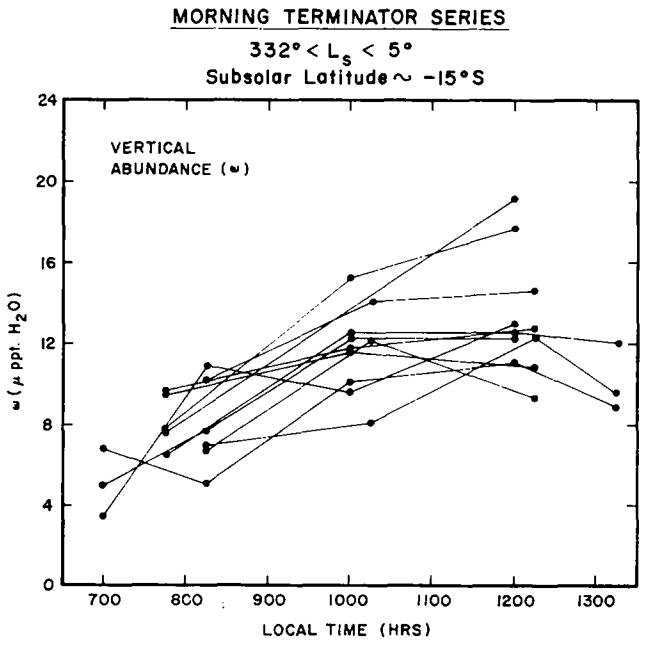

FIG. 10. Vertical H_2O abundances for the morning terminator series.

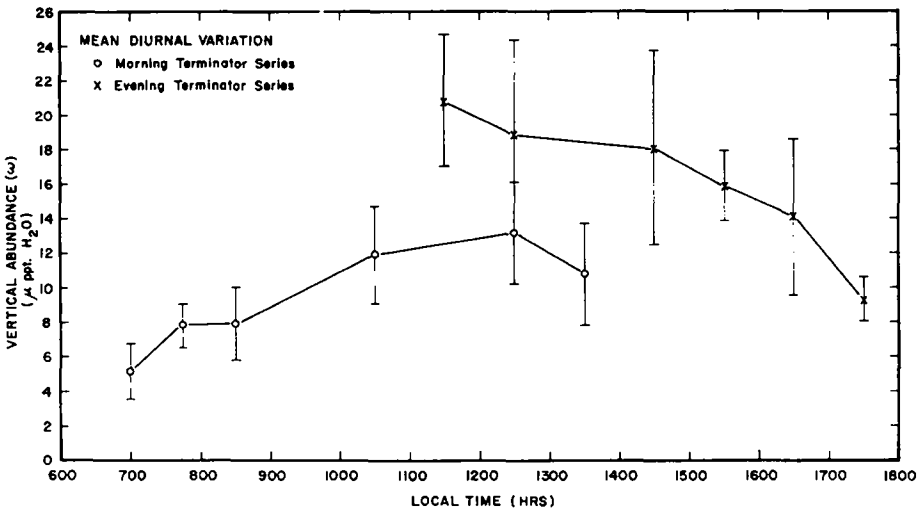

FIG. 11. Mean vertical H_2O abundance from 0700 to 1730 hr, local Martian time.

temperature changes occur in the Martian atmosphere.

In Fig. 12 we show the vertical temperature profiles determined by Mariner 9 (Hanel *et al.*, 1972; Conrath, 1974, personal communication) for a similar season and subsolar latitude as the ground-based water vapor studies. The profiles are for the local times of the maximum and minimum H_2O abundances for both the morning and evening terminator series for an assumed $-3°$/km lapse rate. The dashed portions of the profiles have not been measured and represent approximations to the boundary layer profiles, since the Mariner 9 profiles were not sensitive to these lower regions of the atmosphere. The surface temperatures are taken from the Mariner 9 data (Kieffer *et al.*, 1973) for the same seasonal period as the atmospheric profiles. The temperature profiles show that during the morning terminator series we could have an atmospheric change of about 15 K or a surface temperature change of up to 55 K. In the evening terminator series we could have an atmospheric temperature change of about 5 K and a surface change of about 25 K between midday and 1700 hr. The atmospheric temperature changes in the surface boundary layer are similar but not as large as the surface temperature changes.

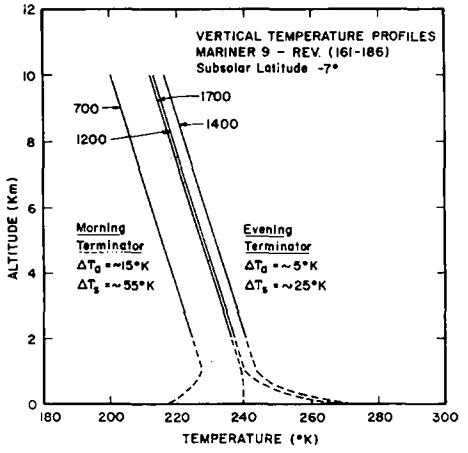

FIG. 12. Vertical atmospheric temperature profiles for interpretation of diurnal H_2O variation.

The evening terminator change of 5 K in the bulk atmospheric temperature above an altitude of 1 km is insufficient to reduce the observed 20 μm abundance to 10 μm by 1700 hr. Consequently, the evening diurnal H_2O abundance decrease must take place in the lower atmosphere (below 1 km).

The morning terminator increase of 15 K in the bulk atmosphere above an altitude of 1 km also is not sufficient to increase the observed 5 μm to 13 μm at 1200 hr, assuming the 5 μm was at or near saturation.

Also, the atmosphere is not cold enough to be saturated with 5 μm unless above 10 km. All these factors imply that diurnal effects take place primarily in the lowest kilometer of the Martian atmosphere.

Since we observe a diurnal effect in the H_2O abundance, some type of condensation—a low ground fog or snow—must take place at night even during the drier seasons on Mars. Only a small fraction of the observed abundance of 20 μm in the form of a condensate (about 2% for particles of 1 μm size) is required to produce an optical depth of unity (Farmer, 1973). The recurrent afternoon brightenings can easily be explained by this mechanism. If the total abundance of 20 μm is precipitated out as frost or snow, an equivalent thickness of 10 to 100 μm for the condensate layer is smaller than the surface roughness scale. Hence, the condensate would not appear as a bright area in the morning especially if the snow had become mixed with the dust layer by nighttime winds.

H_2O Elevation Correlation Analysis

For every abundance measured in the 1972–74 data, an effective elevation was calculated using the same geometrical airmass program (Woodman and Barker, 1973) that was used to calculate the effective airmass for each observation. The elevation above the 6.1 mb areoid at a given point on the disk was convoluted with the seeing profile and weighted by the surface brightness profile. The resulting effective elevation is the average elevation under the slit during the observations. The elevation at a point on the surface was calculated by differencing the shape or topographical surface of the planet using a fourth-degree fit from data presented by Cain (1972, 1973) and the geoid surface using a fourth-degree fit from Jordan and Lorrell (1972, 1975), who used the same base radius of 3393.0 km. The resulting topographic profile relative to an equipotential 6.1 mb is very similar to that

TABLE II

H_2O Elevation Correlation Coefficients r for Each Observational Period and Slit Position

Location	L_s Range (°)	No. of pairs	r	P^a (%)
		Pole to pole		
CM	118–171	29	−0.250	—
CM	185–208	18	−0.093	—
CM	217–250	8	−0.748	97
CM	256–269	3	−0.510	—
CM	328–335	5	−0.814	91
CM	347–5	5	+0.184	—
CM	20–80	16	−0.267	—
		Equatorial		
N/2	185–208	7	−0.534	—
N/2	217–250	9	+0.095	—
N/2	256–269	10	+0.210	—
N/2	328–335	5	−0.876	95
N/2	347–5	9	+0.599	91
N/2	20–80	7	−0.617	93
N/3	328–335	3	−0.636	—
N/3	347–5	3	+0.461	—
N/3	20–80	3	−0.672	—

TABLE II—*continued*

Location	L_s Range (°)	No. of pairs	r	P^a (%)
		Equatorial		
EQ	185–208	10	−0.023	—
EQ	217–250	16	−0.035	—
EQ	256–269	5	−0.845	93
EQ	328–335	7	+0.398	—
EQ	347–5	11	+0.233	—
EQ	20–80	7	+0.146	—
S/2	185–208	7	−0.955	99.9
S/2	217–250	9	+0.311	—
S/2	256–269	8	−0.813	98.5
S/2	328–335	5	+0.716	—
S/2	347–5	7	−0.166	—
S/2	20–80	6	−0.574	—
S2/3	256–269	11	+0.456	—
S. Hem.	139–186	4	−0.396	—
N. Hem.	139–186	5	−0.160	—
		Terminator		
Morn-limb	171–208	11	+0.012	—
Morn-limb	217–250	4	+0.246	—
Morn-limb	256–269	4	−0.937	95
Morn-CD	171–208	15	+0.259	—
Morn-CD	217–250	4	−0.230	—
Morn-CD	256–269	3	−0.013	—
Morn-term	171–208	12	−0.160	—
Morn-term	217–250	4	−0.746	—
Morn-term	256–269	3	+0.874	—
Eve-limb	328–335	3	−0.843	—
Eve-limb	347–5	10	−0.022	—
Eve-L/2	328–335	3	−0.987	90
Eve-CD	328–335	6	−0.129	—
Eve-CD	347–5	11	−0.177	—
Eve-T/2	328–335	4	+0.680	—
Eve-term	328–335	3	−0.160	—
Eve-term	347–5	9	+0.173	—

[a] P is the percent confidence that the observed correlation is not a random number. Missing values are much less than the 90% level, *no* correlation.

presented by Christiansen (1975), who has combined all of the available and pertinent topographic data types.

The Martian water vapor abundances which had adequate spatial resolution, and their corresponding elevations, were tested for any significant level of correlation. By separating the available data into ranges of L_s and type of observation or slit position such as terminator or the N/2 fraction of the disk, we hope to remove any seasonal and diurnal effects shown in previous sections. The majority of the correlation coefficients (r) presented in Table II are not significant, implying a lack of any strong correlation between

abundance and elevation during the seasonal periods with spatial resolution.

In the 48 groups of data, only 9 have any level of significance, ≥90%. Of these 9 groups, only 1 has a positive correlation, the N/2 fraction group just after the dust storm. The other 8 negative correlations mean more water vapor is found over lower elevations; in fact, 6 of the 8 groups have elevations below the 6.1 mb surface. Unfortunately, it was observationally impossible to remove the biases introduced by fixed observing periods and the lack of complete coverage of the entire planet during any one observing run, due to the similar rotation periods of the Earth and Mars.

Based on this fairly uniform sample (greater than 360 abundance measurements during the Martian year and over all central meridians), the amount of water vapor is significantly greater over the lower elevations, and the correlation improves during the wetter seasons which were sampled. Unfortunately, we do not have enough data with spatial resolution at seasons of high water vapor content, such as $L_s = 90$ to 120 and 300 to 330°, to be able to carry out a correlation analysis during these seasons. These gaps should be filled in with 1975–76 observations at McDonald Observatory.

Conclusions

The behavior of water vapor in the atmosphere of Mars can be summarized at this time with conclusions based on spectroscopic observations made at McDonald Observatory during the past several apparitions. All of these abundances and their corresponding physical parameters are available on request for further analysis.

Seasonal. The seasonal behavior of water vapor is similar for the northern and southern hemispheres. The planetwide abundance is low (5 to 15 μm of ppt H_2O) during the equinoctical periods $L_s = 0°$, 180°. The beginning of the return of water vapor to the atmosphere occurs some 60 to 90° of L_s after the spring equinox in each hemisphere. By this time the polar caps have receded to their minimum extent. The southern cap takes about 15° of L_s longer to reach a minimum size and correspondingly the southern hemisphere water vapor increases later than the northern water vapor. This point needs additional observational data with good spatial resolution at $L_s = 60$ to 100° to see if the northern increase takes place at the mid- to high northern latitudes, as it does at $L_s = 265$ to 270° in the southern hemisphere.

The maximum abundance of 35 to 45 μm of ppt H_2O is reached after the summer solstice in each hemisphere. Then during late summer, the abundance decreases to the lower 5 to 15 μm level by the beginning of fall in that hemisphere.

The seasonal behavior of the abundance at any one latitude is very dependent on the insolation at that latitude. We have shown in Fig. 6 that the maximum abundance in the mean N–S distribution follows the subsolar latitude closely, but possibly preceding it by 20° of latitude in the direction of motion.

Dust storm effects. The general seasonal behavior was greatly changed during and after the great dust storms in 1971 and 1973. The global abundances are very low (3 to 8 μm) during a global dust storm and these low values persist even after the dust storm has cleared, indicating not only a masking effect on the lower atmosphere, but more likely an adsorption effect by the dust grains.

Topography effects. The 1972–74 data during the drier seasons (<30 μm) show a negative correlation with effective elevation with respect to the 6.1 mb areoid for 8 of 48 groups of similar sets of measurements. The confidence level of the correlation improves as the seasonal amount of water vapor increases. The confidence levels are not high, but the more important fact is that we only see a negative correlation, meaning more water vapor over a lower terrain.

Diurnal variations. Probably the most significant result of the 1972–74 study is the diurnal change in the water abundance during the drier seasons (5 to 20 μm). A similar effect is to be expected during the wetter seasons when the atmosphere is more saturated, but these seasonal periods were not available during the 1972–74

observing period. The amount of atmospheric water vapor at 0700 hr increases by a factor of 2 to 3× by midday, then decreases by a similar amount by 1700 hr. The diurnal data obtained in the 1972–74 apparition provide constraints for numerical models for the diurnal transport of water across the Martian surface (Flasar and Goody, 1976; Farmer, 1976).

Acknowledgments

The author gratefully acknowledges the many supportive and informative discussions over the several years involved in this project with Drs. Harlan Smith, Ronald Schorn, Barney Farmer, and Robert Tull. Messrs. Michael Perry and Jerry Woodman carried out many observational and computational tasks important to the completion of this paper. Extensive computer reductions and compilations were carried out by Ms. Amber Woodman. This continuing work was supported by NASA NGR 44-012-152.

Note added in proof. More complete and up-to-date information is now available regarding the Mars-3 and Mars-5 water vapor measurements. [*Kosmicheskije Issledovanija* **13**, 33 and 738 (1975)]. The interested reader is referred to the English translation (*Cosmic Research*, Vol. 13, 1976) for details about water vapor amounts from 1 to 125 μm of ppt H_2O.

References

Barker, E. S. (1971). Detection of atmospheric water vapor during the southern hemisphere spring and summer season on Mars. *Bull. Amer. Astron. Soc.* **3**, 277.

Barker, E. S. (1974). Ground-based observations of Mars and Venus water vapor during 1972 and 1973. In *Exploration of the Planetary System: Proceedings of IAU Symposium No.65* (A. Woszczyk and A. Iwaniszewka, Eds.), pp. 111–129. Reidel, Dordrecht, Holland.

Barker, E. S., Schorn, R. A., Woszczyk, A., Tull, R. G., and Little, S. J. (1970). Mars: Detection of atmospheric water vapor during the southern hemisphere spring and summer season. *Science* **170**, 1308–1310.

Baum, W. A. (1974). Results of current Mars studies at the IAU Planetary Research Center. In *Exploration of the Planetary System: Proceedings of IAU Symposium No. 65* (A. Woszczyk and A. Iwaniszewka, Eds.), pp. 241–251. Reidel, Dordrecht, Holland.

Baum, W. A., and Martin, L. J. (1973). Behavior of the Martian polar caps since 1905. *Bull. Amer. Astron. Soc.* **5**, 296.

Cain, D. L., Kliore, A. J., Seidel, B. L., and Sykes, M. J. (1972). The shape of Mars from Mariner 9 occultations. *Icarus* **17**, 517–524.

Cain, D. L., Kliore, A. J., Seidel, B. L., Sykes, M. J., and Woicesyhn, P. (1973). Approximations to the mean surface of Mars and Mars atmosphere using Mariner 9 occultations. *J. Geophy. Res.* **78**, 4352–4354.

Capen, C. F. (1971). Martian yellow clouds—past and future. *Sky & Tel.* **41**, 117–120.

Christensen, E. J. (1975). Martian topography derived from occultation, radar, spectral, and optical measurements. *J. Geophys. Res.* Submitted for publication (preprint).

de Vaucouleurs, G. (1967). A low-resolution photometric map of Mars. *Icarus* **7**, 310–349.

Farmer, C. B. (1971). The strengths of H_2O lines in the 8200 Å region and their application to high dispersion spectra of Mars. *Icarus* **15**, 190–196.

Farmer, C. B. (1976). Liquid water on Mars. *Icarus* **28**, 279–289.

Flasar, F. M., and Goody, R. M. (1976). Diurnal behavior of water on Mars. *Planet. Space Sci.*, **24**, 161–181.

Hanel, R., Conrath, B., Hovis, W., Kunde, V., Lowman, W., McGuire, W., Pearl, J., Pirraglia, J., Prabhakara, C., and Schlachtman, B. (1972). Investigation of the Martian environment by infrared spectroscopy on Mariner 9. *Icarus* **17**, 432–442.

Jansson, P. A., and Korb, C. L. (1968). A table of the equivalent widths of isolated lines with combined Doppler and collision broadened profiles. *J. Quant. Spectrosc. Radiat. Transfer* **8**, 1399–1409.

Jordan, J. F., and Lorrell, J. (1973). Mariner 9: An instrument of dynamical science. Paper presented at the AAS/AIAA Astrodynamics Specialists' Conference, Vail, Colo., July 16–18.

Jordan, J. F., and Lorrell, J. (1975). Mariner 9: An instrument of dynamical science. *Icarus* **25**, 146–165.

Kaplan, L. D., Munch, G., and Spinrad, H. (1964). An analysis of the spectrum of Mars. *Astrophy. J.* **139**, 1–15.

Kieffer, H. H., Chase, S. C., Miner, E., Munch, G., and Neugebauer, G. (1973). Preliminary report on infrared radiometric measurements from the Mariner 9 spacecraft. *J. Geophy. Res.* **78**, 4291–4312.

Kunde, V. G. (1973). Water vapor variations in the atmosphere of Mars from Mariner 9 IRIS. *Bull. Amer. Astron. Soc.* **5**, 297.

LARSON, L. P., FINK, U., AND MICHEL, G. (1973). Infrared spectra of Mars from NASA CV-990 aircraft. *Bull. Amer. Astron. Soc.* **5**, 297.

LITTLE, S. (1971). A report on Martian atmospheric water vapor near opposition, 1969. In *Planetary Atmospheres: Proceedings of IAU Symposium No. 40* (C. Sagan, T. Owen, and H. Smith, Eds.), pp. 241–245. Reidel, Dordrecht, Holland.

MOROZ, V. I., AND KSANFOMALITI, L. V. (1972). Preliminary results of astrophysical observations of Mars from Mars-3. *Icarus* **17**, 408–422.

MOROZ, M. YA., AND PETROV, G. I. (1973). Investigations of Mars from the Soviet automatic stations Mars 2 and 3. *Icarus* **19**, 163–179.

OWEN, T., AND MASON, H. P. (1969). Mars: Water vapor in its atmosphere. *Science* **165**, 893–895.

PEARL, J., CONRATH, B., CURRAN, R., HANEL, R., KUNDE, V., AND PIRRAGLIA, J. (1974). Results from the infrared spectroscopy experiment on Mariner 9. In *Exploration of the Planetary System: Proceedings of IAU Symposium No. 65* (A. Woszczyk and A. Iwaniszewka, Eds.), pp. 293–294. Reidel, Dordrecht, Holland. (Abstract.)

SCHORN, R. A., SPINRAD, H., MOORE, R. C., SMITH, H. J., AND GIVER, L. P. (1967). High-dispersion spectroscopic observations of Mars. II. The water vapor variations. *Astrophys. J.* **147**, 743–752.

SCHORN, R. A., FARMER, C. B., AND LITTLE, S. J. (1969). High-dispersion spectroscopic studies of Mars. III. Preliminary results of 1968–1969 water-vapor studies. *Icarus* **11**, 283–288.

SCHORN, R. A. (1971). The spectroscopic search for water on Mars: A history. In *Planetary Atmospheres: Proceedings of IAU Symposium No. 40* (C. Sagan, T. Owen, and H. Smith, Eds.), pp. 223–236. Reidel, Dordrecht, Holland.

SPINRAD, H., MUNCH, G., AND KAPLAN, L. D. (1963). The detection of water vapor on Mars. *Astrophys. J.* **137**, 1319–1321.

TULL, R. G. (1970). High-dispersion spectroscopic observations of Mars. IV. The latitude distribution of atmospheric water vapor. *Icarus* **13**, 43–57.

TULL, R. G. (1971). The latitude variation of water vapor on Mars. In *Planetary Atmospheres: Proceedings of IAU Symposium No. 40* (C. Sagan, T. Owen, and H. Smith, Eds.), pp. 237–240. Reidel, Dordrecht, Holland.

TULL, R. G. (1972). The coudé spectrograph and echelle scanner of the 2.7 m telescope at McDonald Observatory. ESO/CERN Conference on Auxiliary Instrumentation, Geneva, Switzerland, May 2–5, pp. 259–274.

TULL, R. G., AND BARKER, E. S. (1972). Ground-based photoelectric measures of H_2O on Mars during the Mariner 9 encounter. *Bull. Amer. Astron. Soc.* **4**, 372.

WELLS, D. (1972). The computer-controlled spectrometers at McDonald Observatory. *Publ. Astron. Soc. Pac.* **84**, 203–206.

WOODMAN, J. H., AND BARKER, E. S. (1973). Theoretical calculation of Martian airmass. *Icarus* **19**, 131–136.